

UrbanGraphEmbeddings: Learning and Evaluating Spatially Grounded Vision-Language Embeddings for Urban Environments

Jie Zhang*

National University of Singapore
Department of Architecture
Singapore
jiezhang_jz@u.nus.edu

Xingtong Yu*

The Chinese University of Hong Kong
Dept of Systems Eng. & Eng. Mgmt.
China
xtyu@se.cuhk.edu.hk

Yuan Fang†

Singapore Management University
School of Computing & Info. Systems
Singapore
yfang@smu.edu.sg

Rudi Stouffs†

National University of Singapore
Department of Architecture
Singapore
stouffs@nus.edu.sg

Zdravko Trivic†

National University of Singapore
Department of Architecture
Singapore
akitz@nus.edu.sg

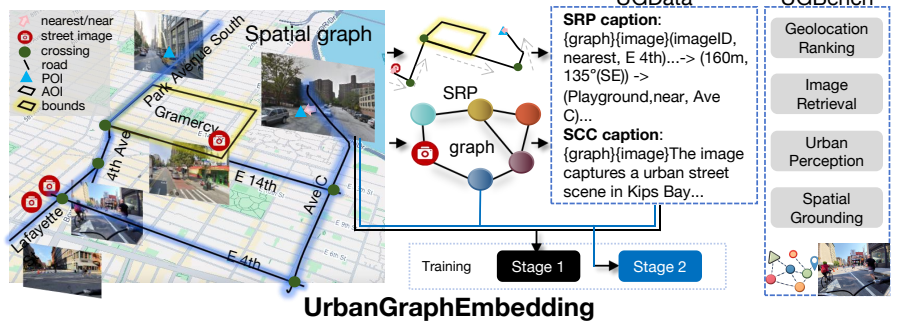


Figure 1: Comparison between existing urban VLM approaches and URBANGRAPHEMBEDDING. Existing methods mainly rely on QA-style supervision and image–text alignment, whereas URBANGRAPHEMBEDDING aligns images, text, and spatial graphs to learn and evaluate spatially grounded urban representations using UGData and UGBench.

Abstract

Learning transferable multimodal embeddings for urban environments is challenging because urban understanding is inherently spatial, yet existing datasets and benchmarks lack explicit alignment between street-view images and urban structure. We introduce UGDATA, a spatially grounded dataset that anchors street-view images to structured spatial graphs and provides graph-aligned supervision via spatial reasoning paths and spatial context captions, exposing distance, directionality, connectivity, and neighborhood context beyond image content. Building on UGDATA, we propose UGE, a two-stage training framework that progressively and stably aligns images, text, and spatial structures by combining

instruction-guided contrastive learning with graph-based spatial encoding. We finally introduce UGBENCH, a comprehensive benchmark to evaluate how spatially grounded embeddings support diverse urban understanding tasks—including geolocation ranking, image retrieval, urban perception, and spatial grounding. We develop UGE on multiple state-of-the-art VLM backbones, including Qwen2-VL, Qwen2.5-VL, Phi-3-Vision, and LLaVA1.6-Mistral, and train fixed-dimensional spatial embeddings with LoRA tuning. UGE built upon Qwen2.5-VL-7B backbone achieves up to 44% improvement in image retrieval and 30% in geolocation ranking on training cities, and over 30% and 22% gains respectively on held-out cities, demonstrating the effectiveness of explicit spatial grounding for spatially intensive urban tasks. The code and datasets are available at <https://github.com/Jayagaga/UGE/tree/main>.

*Co-first authors.

†Corresponding authors.

Permission to make digital or hard copies of all or part of this work for personal or classroom use is granted without fee provided that copies are not made or distributed for profit or commercial advantage and that copies bear this notice and the full citation on the first page. Copyrights for components of this work owned by others than the author(s) must be honored. Abstracting with credit is permitted. To copy otherwise, or republish, to post on servers or to redistribute to lists, requires prior specific permission and/or a fee. Request permissions from permissions@acm.org.

Conference acronym 'XX, Woodstock, NY'

© 2018 Copyright held by the owner/author(s). Publication rights licensed to ACM.

ACM ISBN 978-1-4503-XXXX-X/2018/06

<https://doi.org/XXXXXX.XXXXXXX>

CCS Concepts

- Information systems → Information retrieval; • Computing methodologies → Artificial intelligence.

Keywords

Urban computing, multimodal learning, spatial graphs

ACM Reference Format:

Jie Zhang*, Xingtong Yu*, Yuan Fang[†], Rudi Stouffs[†], and Zdravko Trivic[†]. 2018. UrbanGraphEmbeddings: Learning and Evaluating Spatially Grounded Vision–Language Embeddings for Urban Environments. In *Proceedings of Make sure to enter the correct conference title from your rights confirmation email (Conference acronym 'XX)*. ACM, New York, NY, USA, 17 pages. <https://doi.org/XXXXXX.XXXXXXX>

1 Introduction

Urban science is increasingly powered by learning representations from multi-source urban observations, ranging from street-level imagery, remote sensing data, geo-text, to 3D point clouds and spatiotemporal trajectories. This has led to a growing reliance on vision–language models (VLMs) [14, 18] as a general-purpose backbone for urban representation learning. By pre-training on large-scale image–text corpora to acquire transferable multimodal alignments, these models can be directly reused or lightly adapted to support a wide range of urban tasks, such as geolocation prediction [7, 10, 17, 52], socioeconomic indicator prediction [35], navigation prediction [45, 59], spatial reasoning [14, 53] and urban scene understanding [8, 43].

However, urban understanding is not simply visual and textual, but spatial and relational. The semantics of a location is not solely determined by what is visible in a single street-view image or expressible in a local caption, but also by how the location is positioned within the city’s topology, such as its connectivity, proximity, and broader neighborhood structure [12, 38]. As shown in Fig. 1, current urban VLMs rely on instruction tuning and QA-style supervision, encoding spatial information implicitly through language and confining it to isolated question contexts, resulting in fragmented, task-specific representations that lack explicit urban grounding. This limitation stems from the lack of datasets that explicitly align spatial knowledge with images and texts, leaving urban VLMs to optimize primarily for visual–textual alignment without an explicit pathway to encode geographic structure beyond the camera’s field of view. This gap motivates the creation of a benchmark that enhances urban VLM fine-tuning and evaluation by integrating urban spatial data to better capture spatial relationships. However, this is non-trivial due to two key challenges.

First, *how to extract spatial knowledge and align with street-level images, capturing urban relationships beyond what is directly visible?* Urban spatial knowledge is inherently structured, heterogeneous, relational, and multi-scale, and cannot be adequately captured by isolated image–text pairs. Moreover, effective supervision for spatial representation learning must be compatible with existing VLM training paradigms. To address this challenge at the data level, we leverage urban spatial graphs [25, 27, 56], which use low-cost, large-scale open geographic data to model locations as nodes connected by roads and functional relations. From such spatial graphs, we construct **UGDATA**, a spatially grounded dataset that explicitly anchors each street-view image to its surrounding urban context. Specifically, for each image, we assign a localized spatial subgraph and derive structured, language-aligned supervision signals, including *spatial reasoning paths* (SRPs) and *spatial context captions* (SCCs), describing how the image location is situated within the broader urban environment. UGDATA pipeline is low-cost and highly scalable, with supervision grounded in reliable geographic data rather than

manual annotation. Building on this pipeline, we treat spatial graph as a standalone input modality aligned with street-level images, enabling multimodal embedding learning that captures structured urban context beyond visual appearance alone.

Second, *how can structured spatial knowledge be progressively injected into VLM embeddings in a stable and transferable manner, enabling general-purpose spatial representations?* Naively combining images, text, and spatial graphs during training can lead to unstable optimization, as pretrained visual–language representations can be sensitive to distribution shifts introduced by an additional modality. Hence, we propose a two-stage training framework, **URBANGRAPHEMBEDDING**, that progressively injects spatial knowledge into VLM embeddings while preserving their visual–language alignment. Specifically, spatial awareness is first induced via textual spatial reasoning cues in Stage 1, followed by explicit urban spatial structure encoding in Stage 2 through a graph encoder that propagates topological and relational information from spatial subgraphs.

To evaluate the learned representations, we introduce **UGBENCH**, a benchmark that assesses performance across various urban science tasks: geolocation ranking, image retrieval, urban perception, and spatial grounding. It adopts a unified embedding-based ranking framework, supporting mono-modal or graph-augmented inputs under zero-shot evaluation.

In summary, our contributions are threefold: (1) We introduce a spatially grounded urban dataset with spatial reasoning paths and spatial context captions that explicitly align street-view images with graph-structured urban context. (2) We propose a two-stage training strategy that progressively injects structured spatial knowledge into VLM embeddings via instruction-guided contrastive learning and graph-conditioned encoding. (3) We present a systematic benchmark that evaluates spatial representations in a zero-shot setting, assessing whether spatial context improves retrieval and ranking across diverse urban science tasks.

2 Related Work

Urban Datasets and Benchmarks. Existing urban datasets and benchmarks target specific aspects of spatial understanding, such as navigation [4], urban scene understanding [9, 23], urban perception [21, 44], geolocation prediction [17, 19, 52], and land-use analysis [49]. While effective for task-specific learning, these datasets lack explicit alignment between images, text, and urban spatial structure. CityBench [15] evaluates LLMs across diverse urban tasks, revealing limitations in spatial reasoning. UrbanLLaVA [14], CityCube [54], SpatialLab [51], and InternSpatial [11] assess VLMs’ spatial reasoning ability through QA-style tasks largely confined to the camera’s observable field. DynamicVL [55] and URBANFEEL [20] focus on dynamic and perceptual city understanding, while GeoBenchX [30] and GeoChain [57] evaluate multi-step geographic reasoning and expose LLM/VLMs’ weaknesses in spatial inference. Overall, existing urban datasets and benchmarks remain task-centric and underexplore the quality of learned spatial representations. In contrast, we propose a spatially grounded training dataset, together with a representation-centric benchmark that evaluates how well multimodal embeddings encode and align urban spatial knowledge across modalities.

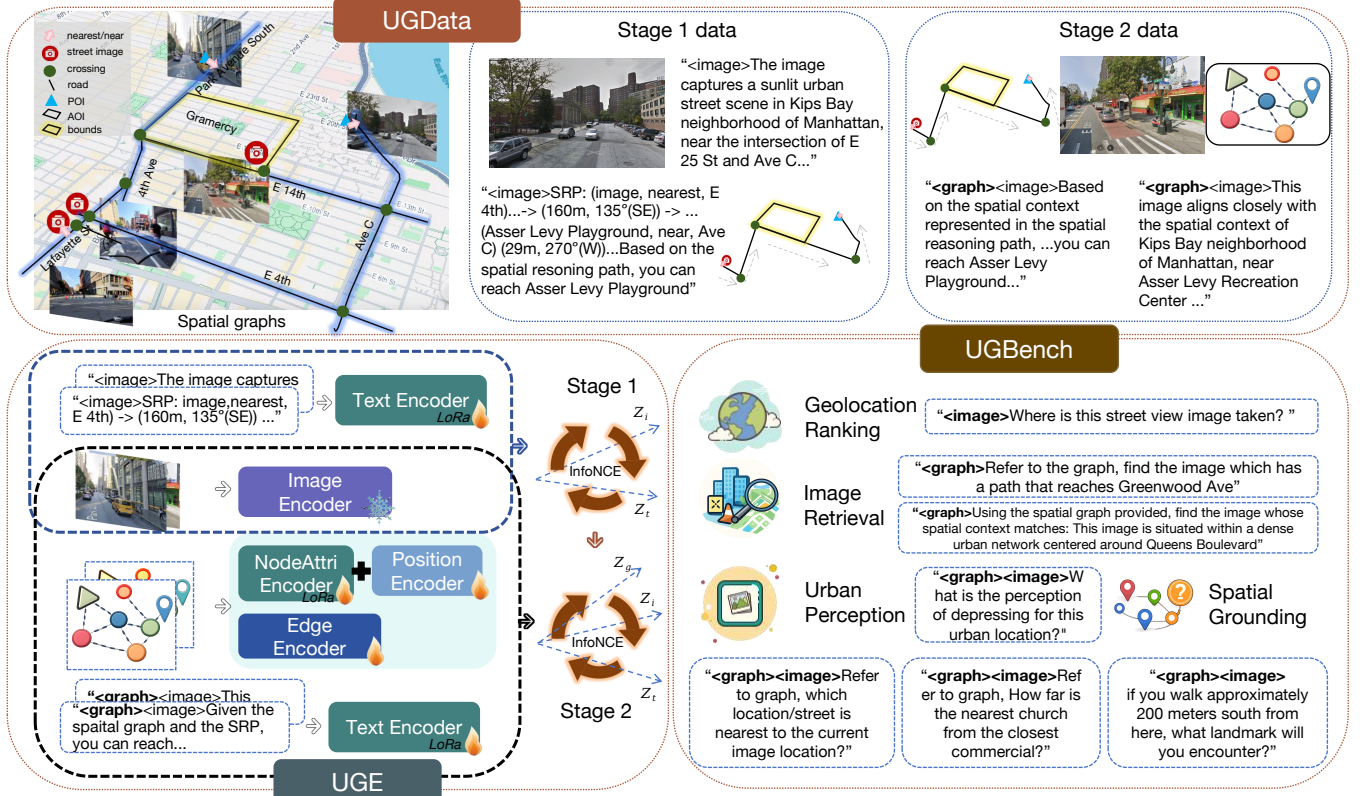


Figure 2: Overview of the URBANGRAPEMBEDDING framework.

Multimodality Learning. Recent visual language models (VLMs) such as LLaVA and Qwen-VL achieve strong visual understanding via large-scale instruction tuning, while multimodal embedding models extend CLIP-style alignment toward more general representation spaces that accommodate diverse modalities. Approaches including GME[60], jina-embeddings-v4 [16], and VLM2Vec/VLM2Vec-V2 [28, 41] use contrastive training to learn transferable embeddings across images, text, and other multimodal content. Despite the progress, both VLMs and general-purpose multimodal embeddings predominantly encode visual, semantic, or layout-level patterns, while lacking explicit representations of geographically embedded structure such as connectivity and topology, which limits their applicability to urban tasks that require spatial understanding beyond local visual cues. The absence of datasets and benchmarks with explicit spatial structure also constrains systematic training and evaluation of such capabilities of VLMs.

Graph-based Spatial Encoding for Urban Knowledge. A complementary line of work enhances LLM and VLM reasoning by grounding models in structured relational data such as knowledge graphs (KG) and text-attributed graphs. [26, 31, 42, 48] demonstrated that visual-textual knowledge graphs enable relational grounding. GCR[37] has showed that graph-constrained reasoning improves faithfulness and interpretability in language-centric settings. [22] introduced geometric KG embeddings that incorporate spatial cues for structured reasoning but was not designed for urban-scale multimodal alignment. Recent frameworks such

as SpatialRGPT [5] and SpatialRAG [58] leveraged structured spatial information for question answering and reasoning, yet treat spatial structure as auxiliary context rather than a representation modality aligned with visual perception. In parallel, Structure-CLIP [24] showed that graph-conditioned learning can enhance vision-language embeddings, though it focused on object-centric scene graphs rather than geographic structure. Prior GeoAI work applied graph encoders to model distance, direction, and topology [6, 29, 32]. Collectively, these studies motivate the explicit integration of graph-structured spatial priors into VLMs, enabling spatially aware multimodal embeddings that generalize across diverse urban science tasks.

3 URBANGRAPEMBEDDING

In this section, we present URBANGRAPEMBEDDING (UGE). As illustrated in Fig. 2, the UGE framework integrates spatially grounded training data (UGDATA), a progressive two-stage learning strategy, and a unified benchmark for evaluating urban spatial representations (UGBENCH). We introduce these components in turn.

3.1 UGDATA: Training Data Pipeline

3.1.1 Urban Spatial Graph Construction. We construct city-scale spatial graphs by integrating street-level imagery from Mapillary¹

¹<https://www.mapillary.com/>

Table 1: Urban spatial graph schema.

Category	Type	Description
Node	Street-level viewpoint	Street-view image location
	Road	Road
	Intersection	Junction of roads
	POI	Point of Interests
	AOI	Area of Interests
Edge	Transit Facility	Metro station, bus stop, etc.
	on_same_street	Two POIs on the same road
	crossing	Junction points of roads
	nearest	POI's nearest road
	near	A road is near to a POI
	bounds	A road bounds AOI
	intersects	A road intersects AOI

with urban entities extracted from OpenStreetMap², further augmented by open municipal datasets covering buildings, green space, historic districts, and transportation³. In this graph, nodes represent street-view images or urban entities, while edges encode spatial relations (Table 1), capturing accessibility and connectivity to support spatial reasoning. This spatial graph is naturally scalable, allowing new entities to be incorporated via local spatial relations without global reconstruction.

Based on the spatial graphs, we derive *spatial reasoning paths* (SRPs) for Stage 1 training and *spatial context captions* (SCCs) for Stage 2 graph-conditioned training, as follows.

3.1.2 Spatial Reasoning Paths. A key challenge in spatially aware multimodal learning is bridging structured urban graphs with the language-centric reasoning of VLMs. To address this, we introduce Spatial Reasoning Paths (SRPs), which extend reasoning paths in RoG [36] and GCR [37] by revealing relative distance and direction and organizing graph triples into a sequence of waypoints for navigation-based spatial alignment. This design is motivated by cognitive theories showing that human form mental maps through relational and hierarchical structures centered on nodes, paths, and landmarks rather than isolated locations [38, 40, 46, 47].

Specifically, an SRP is an ordered sequence of relational triples (e_s, r, e_t) , capturing semantic and topological relations (e.g., nearest, crossing), interleaved with transition tuples (d, θ) that encode geodesic distance and relative direction between consecutive entities based on geographic coordinates and network geometry. An example SRP is shown below:

```
((imageID), nearest, Robert F. Kennedy Bridge)(10.6 m, 52°NE)
(789.0 m, 143°SE) → (Robert F. Kennedy Bridge, crossing, 21st St)
(310.1 m, 223°SW) → (21st St, near, NY Ctr. for Rehab & Nursing)(28.5 m, 128°SE).
```

From the image location, the path links to the Robert F. Kennedy Bridge (10.6 m northeast), follows the road southeast for 789 m to the bridge–21st Street crossing, and reaches NY Center for Rehab & Nursing, 28.5 m southeast of 21st Street, as illustrated in Fig. 3(a).

In implementation, we generate SRPs via S2-based partitioning⁴ and localized graph traversal. See Appendix D for SRP generation details. We also include brief instructional text accompanying each

²<https://www.openstreetmap.org/>

³<https://opendata.cityofnewyork.us/>, <https://data.gov.sg/>

⁴S2 is a spherical geometry library for representing geographic data and building spatial indexes (<https://s2geometry.io/>).

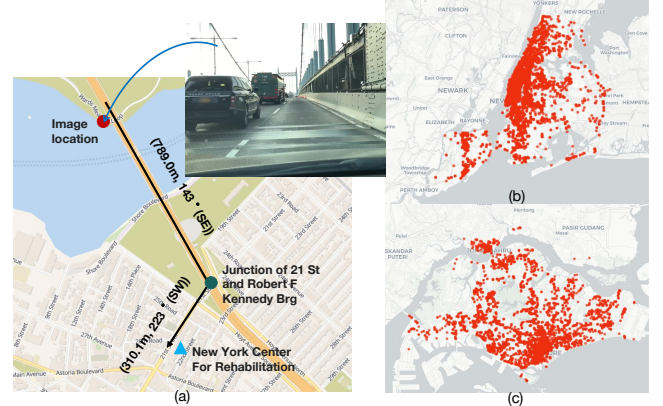


Figure 3: Overview of spatial context and data coverage: (a) Map illustration of an SRP; (b), (c) Street-view image distributions in New York and Singapore.

SRP to indicate how the path should be interpreted from a user perspective (e.g., reachability, facing direction, and viewpoint), guiding the model to ground the path in both the image and spatial graph. See examples in Appendix A.

3.1.3 Spatial Context Captions. While SRPs focus on individual paths originating from the image location, they lack a holistic representation of the surrounding neighborhood. To capture such a holistic view, thereby better aligning street-level images with their spatial graphs, we generate Spatial Context Captions (SCCs) that integrate visual cues with graph-derived semantic and relational information. For each image, a localized spatial subgraph is summarized as structured context and, together with the image, provided to an LLM (GPT-4.1 and Qwen-VL-Max-Latest) to generate a spatially grounded natural-language caption⁵ (see details and examples in Appendix A, B, C). These captions jointly capture what is visible in the image and how the location is situated within its urban neighborhood.

3.1.4 Data Statistics. Our dataset is built on city-scale spatial graphs from New York, Singapore, Beijing, and Paris, with New York and Singapore used for training and Beijing and Paris reserved for cross-city evaluation. The spatial graphs for New York and Singapore contain 487K and 338K nodes and 7.3M and 333K edges, respectively. From the two training cities, we construct 17,736 SRPs (average 7.27 hops) and generate 8,039 SCCs, comprising 92,612 entity mentions over 20,838 unique entities. These graph-derived signals are used to construct supervision at different stages of training: *Stage 1* includes 44,356 image–text samples (SRPs and image-level captions), while *Stage 2* consists of 25,775 graph-conditioned samples (SRPs and SCCs with graphs). The spatial distribution of street-view images in the training cities is shown in Fig. 3(b,c). Overall, our dataset pipeline is scalable, extensible, and reproducible. Next, we introduce the two-stage progressive training strategy using our data.

⁵The captioning model is instructed to rely strictly on the provided subgraph description and not introduce external or fabricated spatial information.

3.2 Two-Stage Training

While SRPs and SCCs provide spatially grounded supervision at the data level, effectively incorporating structured spatial knowledge into VLM embeddings poses additional challenges at the model and optimization level. First, urban spatial knowledge is heterogeneous and structured, involving connectivity, topology and neighborhood context that are not explicitly encoded in standard image–text pairs. Second, directly injecting such knowledge through task-level supervision often leads to representations that do not generalize well across retrieval, ranking, and reasoning settings. Finally, naïvely mixing visual, textual, and graph-structured signals during training can lead to unstable optimization and under-utilization of spatial structure. To address these challenges, we adopt a two-stage training strategy tailored to spatial VLM embedding learning (Fig. 2).

3.2.1 Stage 1: Instruction-Guided Image–Text Alignment. In the first stage, we perform *instruction-guided contrastive embedding learning* to align images with spatially enriched textual descriptions, including *SRPs* and *image-level captions*. Beyond generic image–text alignment, this stage injects structured spatial knowledge into the visual–language embedding space by grounding images in local spatial context expressed through language, following the contrastive paradigm of VLM2Vec [28].

Let (q, t^+) denote a positive query–target pair, where the query q is a street-level image and the target t^+ is a textual description.

Instruction construction. Given an image query q_i , we construct an instruction-augmented query q_{inst} as:

$$q_{\text{inst}} = [\text{IMAGE_TOKEN}] \text{ Instruct: } \{\tau\}, \quad (1)$$

where τ is a fixed, task-agnostic instruction selected according to the target type. Specifically, we use two instruction templates:

τ_{path} : “Describe whether the {destination} is reachable from this viewpoint.”
 τ_{cap} : “Provide a detailed description of the image content.”

These instructions guide the model to interpret the image either in terms of *navigability and spatial relations* or *visual semantics*.

Contrastive objective. We optimize the embeddings using the standard InfoNCE loss over in-batch negatives:

$$\mathcal{L}_{\text{Stage1}} = -\log \frac{\phi(\mathbf{h}_{q_{\text{inst}}}, \mathbf{h}_{t^+})}{\phi(\mathbf{h}_{q_{\text{inst}}}, \mathbf{h}_{t^+}) + \sum_{t^- \in \mathcal{N}} \phi(\mathbf{h}_{q_{\text{inst}}}, \mathbf{h}_{t^-})}, \quad (2)$$

where \mathcal{N} denotes in-batch negative text samples and $\phi(\cdot, \cdot)$ is a similarity function (cosine similarity with temperature scaling).

3.2.2 Stage 2: Graph-Conditioned Spatial Embedding. In the second stage, we introduce a *graph encoder* that explicitly conditions street-view image embeddings on their associated local spatial graphs, enabling alignment with structured urban spatial context. We again consider a positive pair (q, t^+) . In Stage 2, the query is *multimodal*, consisting of a street-level image and its associated spatial graph, while the target remains text-based (SRPs or SCCs).

Instruction construction with graph tokens. Given an image q_i and its corresponding spatial subgraph q_g , we construct

an instruction-augmented multimodal query:

$$q_{\text{inst}} = [\text{GRAPH_TOKEN}] [\text{IMAGE_TOKEN}] \text{ Instruct: } \{\tau\}, \quad (3)$$

where τ is a fixed instruction selected according to the target type. We use two instruction templates in Stage 2:

τ_{path} : “Refer to the image and spatial graph, describe the pedestrian navigation context and spatial paths from this viewpoint.”
 τ_{ctx} : “Use the image and graph together to describe the scene and its spatial context.”

Progressive injection. We apply the same InfoNCE loss for Stage 2, as introduced in Eq. (2). To preserve the visual–language alignment learned in Stage 1, we train the graph encoder with a higher learning rate while updating VLM parameters conservatively, allowing spatial structure to be injected without disrupting visual grounding. This staged design decouples semantic alignment from spatial regularization and supports flexible inference with or without graph input, yielding transferable multimodal embeddings. We next introduce the graph encoder used in Stage 2.

3.2.3 Graph Encoder (for Stage 2). The graph encoder is composed of a node encoder and an edge encoder, designed to encode localized urban subgraphs surrounding each street image. The graph encoder transforms spatial entities and their pairwise spatial relations into embeddings that can be fused with image representations for graph-conditioned contrastive learning.

Node encoder. Each node is associated with textual attributes (e.g., name, category, address) and geographic coordinates. Textual attributes are encoded using the shared language embedding layer of the VLM. To encode spatial position, we apply a multi-frequency sinusoidal spatial positional encoding over longitude–latitude coordinates, following the design principles of PE-GNN[29]. The textual and spatial embeddings are concatenated and projected to obtain the final node embedding.

Edge encoder. Edges encode explicit geodesic and spatial relationships between nodes, capturing how urban entities are positioned and connected in physical space. For each edge, we construct three complementary spatial features: (1) relative distance, computed as the log-transformed haversine distance; (2) relative direction, represented by sine and cosine of the bearing angle; (3) relative displacement, given by the coordinate offset between nodes. These features are jointly embedded through a learnable edge encoder.

Graph message passing. We adopt GATv2[3] conditioned on learned edge features encoding spatial relations, enabling multi-layer propagation of spatial context with residual connections and layer normalization.

3.3 UGBench: Evaluating Urban Tasks

We introduce the **UGBENCH** benchmark, which evaluates spatially informed VLM embeddings across four tasks: *geolocation ranking*, *image retrieval*, *urban perception*, and *spatial grounding*. An overview of the benchmark is provided in Table 2.

All tasks in UGBENCH are formulated as *embedding-based ranking problems*, following VLM2Vec [28]. Each instance provides an instruction and a query (text, image, or image with graph context),

Table 2: Overview of UGBENCH tasks and dataset statistics.

Task	Query	Target	#Cand.	NY	SG	BJ	PA
Geolocation	I	T	20	260	260	260	260
Urban Perception	Safe, Wealthy, Lively, Depressing, Boring, Beautiful	I	20	389	389	389	389
Image Retrieval	T / T+G	I	20	700	700	700	700
Spatial Grounding							
Nearest Street	I / I+G	T	20	600	600	600	600
Nearest POI	I / I+G	T	20	260	260	260	260
Distance	I / I+G	T	20	260	260	260	260
Distance-Direction	I / I+G	T	20	260	260	260	260

I/T/G denotes image/text/spatial graph queries; I+G/T+G indicates multimodal combinations.

and both queries and candidates are embedded into a shared space using the last-layer hidden state of the final token. Candidates are then ranked by cosine similarity to the query embedding. Detailed descriptions of each task follow.

3.3.1 Geolocation Ranking. Unlike conventional geolocation benchmarks that predict coordinates or coarse regions, our geolocation ranking task uses *fine-grained textual descriptions of local spatial context* as labels, capturing hierarchical and relational cues such as street names, intersections, nearby landmarks, and neighborhoods anchored to precise coordinates.

Example. *Query:* “[graph] Where is this street view image taken? Select the correct location.” *Candidates:* “on Union St, near the intersection of 5 Ave and Union St, in Park Slope, Brooklyn, ...”

What it tests. This task evaluates fine-grained, hierarchical, and relational location understanding beyond coordinate or region prediction.

3.3.2 Image Retrieval. The task is to retrieve relevant street view images given a textual query augmented with spatial graph context.

Example. *Queries:* “[graph] Which street view image references a journey ending at 248, Central Park West?”, “[graph] Using the spatial graph provided, find the image whose spatial context matches: This image is situated within a dense urban network centered around Queens Boulevard...” *Candidates:* 21 Mapillary images from the same city corpus.

What it tests. This task evaluates cross-modal alignment between textual semantics, structured spatial context, and visual content, and whether explicit spatial structure improves retrieval beyond text alone.

3.3.3 Urban Perception. This benchmark extends *Global Streetscapes* [21] by augmenting each street-view image with its associated *local spatial graph*. Human-annotated perception scores (safety, wealthiness, liveliness, beauty, boredom, and depressiveness) are discretized into fine-grained textual categories, and the task is to rank these labels given an image and its spatial graph. For evaluation, we randomly sample 389 held-out instances from New York and Singapore after excluding training locations.

Example. *Query:* “[graph]{image} Given the spatial graph, what is the perception of wealthiness for this image location?” *Candidates:* “Very wealthy, Wealthy Score: 9.0,” “Moderately wealthy, Wealthy Score: 6.5, ...” **What it tests.** This task evaluates whether embeddings capture higher-level urban semantics that are not fully determined by local visual appearance and may benefit from broader spatial context.

3.3.4 Spatial Grounding. Compared to previous spatial reasoning benchmarks [11, 13, 14, 54], our spatial grounding task does not supervise explicit answer generation, but evaluates whether spatial structure underlying *daily experience* is internalized in the

embedding space to support retrieval and transfer across urban tasks. Queries and candidates are derived from a *local spatial graph anchored at a street-view image location* and span three types: (1) proximity queries, (2) distance-sensitive queries based on relative distance, and (3) compositional distance-direction queries involving directionality and multi-hop relations.

Examples.

- **Nearest street:** “[graph]{image} Using the provided spatial graph, what street is this location on or nearest to?”
- **Nearest POI:** “[graph]{image} Using the provided spatial graph, which POI is nearest to the current image location?”
- **Distance:** “[graph]{image} How far is the nearest church from the closest commercial?”
- **Distance-direction:** “[graph]{image} Refer to the spatial graph, if you walk approximately 200 meters south from here, what landmark will you encounter?”

What it tests. This benchmark evaluates whether spatial reasoning concepts, such as proximity, distance, directionality, and multi-hop relations, are implicitly reflected in the embedding space to enable spatially informed retrieval.

4 Evaluation and Benchmarking

In this section, we conduct experiments to evaluate UGE, and analyze the empirical results.

4.1 Experimental Setup

Task evaluation. All evaluations are conducted in a zero-shot setting. We report Hit@5 and NDCG@5⁶ for all tasks. Note that our ranking candidates are intentionally constructed to be spatially or semantically plausible, reflecting real-world urban settings.

Baselines. We compare against strong vision–language models and multimodal embedding models to evaluate the effectiveness of our spatial data and two-stage training strategy. The VLM baselines include Qwen2-VL (2B/7B) [50], Qwen2.5-VL (3B/7B) [2], Phi-3-Vision-128K [1], and LLaVA1.6-Mistral [33]. Multimodal embedding models include GME-Qwen2VL-2B-Instruct [60] and VLM2Vec-Qwen2VL-2B [28].

Implementation and training details. All models are fine-tuned and evaluated using the *Swift* framework⁷, with LoRA adapters and DeepSpeed for efficient finetuning. More details about finetuning can be found in Appendix F.

4.2 Benchmarking Performance on UGBench

Overall performance. As shown in Tables 3 and 4, spatial graph-enhanced fine-tuning consistently improves ranking performance, as measured by both Hit@5 and NDCG@5 across geolocation ranking, image retrieval, urban perception, and spatial grounding tasks. These gains are observed across all four cities, demonstrating strong generalization to held-out cities (Beijing and Paris), despite training only on New York and Singapore, with larger improvements generally seen in training cities. GME and VLM2Vec exhibit stronger zero-shot performance than their corresponding

⁶Hit@5 measures whether correct candidates are prioritized among the top results, while NDCG@5 evaluates the quality of the ranking within the top positions.

⁷ms-swift is a large-model fine-tuning and deployment framework provided by the ModelScope community. <https://github.com/modelscope/ms-swift>.

Table 3: Results on geolocation ranking, image retrieval, and urban perception. Urban perception is averaged over 6 attributes listed in Table 2; results for each individual attribute are reported in Appendix G. H@5: Hit@5, N@5: NDCG@5, in percent.

Model	Geolocation Ranking								Image Retrieval								Urban Perception (Avg.)															
	NY				SG				BJ				PA				NY				SG				BJ				PA			
	H@5		N@5		H@5		N@5		H@5		N@5		H@5		N@5		H@5		N@5		H@5		N@5		H@5		N@5					
Qwen2-VL-2B	29.23	14.86	34.23	18.26	44.62	24.50	45.00	24.49	32.00	19.47	29.29	17.77	34.14	20.77	30.14	17.38	22.75	13.09	21.20	12.51	23.53	13.31	24.08	14.85								
UGE	44.23	30.98	48.85	36.04	71.92	64.18	61.15	42.80	55.57	39.36	62.23	45.72	62.57	40.61	49.07	33.42	31.47	18.60	26.98	16.32	23.90	13.53	26.40	16.08								
Qwen2-VL-7B	27.31	17.16	35.00	22.93	59.62	50.66	30.00	18.37	31.57	18.69	28.29	16.98	36.86	22.56	30.00	18.42	16.80	8.45	24.33	13.60	27.38	17.61	22.45	11.50								
UGE	55.00	39.30	49.62	35.26	65.77	54.93	48.85	31.24	65.43	47.32	70.10	52.44	56.29	39.06	49.07	34.12	31.96	18.02	29.52	17.47	25.75	14.51	27.89	16.22								
Qwen2.5-VL-3B	19.23	11.76	30.00	17.85	20.77	13.16	0.38	0.19	26.71	15.86	26.00	15.76	27.43	16.73	24.29	15.29	24.48	14.95	20.57	12.20	16.82	8.81	20.61	12.26								
UGE	37.69	23.93	36.92	26.83	56.92	49.15	40.77	28.84	47.43	31.12	45.06	30.33	44.29	29.50	36.05	22.68	25.48	14.75	26.18	15.59	21.42	13.63	26.48	15.44								
Qwen2.5-VL-7B	32.69	20.24	33.85	21.43	48.08	36.01	39.62	26.83	33.71	21.21	26.57	15.97	27.14	15.98	31.71	18.98	20.44	11.18	26.18	15.00	27.08	16.75	23.82	13.32								
UGE	58.85	47.94	64.23	54.65	71.92	63.38	65.77	52.88	58.86	43.24	71.10	52.22	57.43	40.44	57.22	41.50	41.69	27.12	35.35	23.68	34.17	22.71	40.59	26.81								
GME-2B	29.23	14.86	34.23	18.26	44.62	24.50	45.00	24.49	42.43	22.78	47.29	25.60	53.14	28.70	44.00	23.56	28.03	14.26	28.24	13.85	30.04	14.63	26.57	12.94								
UGE	41.15	28.68	46.15	33.15	46.54	32.20	54.62	37.81	55.43	41.16	60.37	44.10	59.14	40.80	51.65	36.06	25.04	13.12	30.24	17.52	20.91	12.60	19.19	10.76								
VLM2Vec-2B	30.77	18.54	34.23	22.06	43.85	33.82	56.15	34.97	52.57	36.30	56.43	42.17	59.29	43.72	54.00	37.50	18.27	9.01	18.59	8.76	18.92	8.86	19.02	9.21								
UGE	48.85	31.64	47.69	33.79	39.23	29.08	50.00	34.50	54.57	38.67	63.52	45.59	58.29	38.52	48.93	33.01	31.02	17.56	25.24	14.88	24.43	13.66	25.07	14.21								
LLaVA1.6	28.85	17.73	26.15	14.80	22.69	14.77	20.00	11.48	29.71	17.60	29.29	18.22	32.29	18.74	28.00	16.98	29.01	17.50	23.39	13.85	24.64	14.75	24.55	13.75								
UGE	53.46	35.13	55.38	38.06	48.08	37.64	56.92	39.54	41.50	28.64	39.41	27.59	31.50	18.27	46.92	30.96	35.54	21.19	24.52	14.22	23.35	13.91	24.11	13.75								
Phi3-V	24.62	13.53	28.85	17.30	38.46	28.67	18.85	12.16	36.29	21.04	36.14	23.04	31.00	19.65	31.00	18.57	27.16	15.04	31.79	18.21	24.12	13.74	25.96	14.73								
UGE	39.23	23.70	43.85	30.96	51.92	43.14	58.46	41.36	45.43	29.73	47.93	30.24	48.43	31.11	41.34	26.26	28.55	16.17	23.31	13.46	27.68	16.66	27.68	16.07								

Table 4: Spatial grounding results across query types and cities. Results of Nearest Location is reported in Appendix H.

Model	Nearest POI								Distance								Distance-Direction															
	NY				SG				BJ				PA				NY				SG				BJ				PA			
	H@5		N@5		H@5		N@5		H@5		N@5		H@5		N@5		H@5		N@5		H@5		N@5		H@5		N@5					
Qwen2-VL-2B	39.44	29.72	45.38	42.44	66.92	58.65	26.92	19.29	12.31	11.01	18.85	16.90	27.69	26.09	23.46	22.06	26.09	24.99	23.46	22.06	40.00	39.40	36.54	35.15								
UGE	45.07	37.18	60.00	55.77	72.31	66.75	30.77	20.08	21.92	21.70	29.23	28.23	31.92	30.45	25.00	24.76	33.04	32.04	26.54	26.30	41.92	39.80	45.00	40.40								
Qwen2-VL-7B	36.15	29.19	38.46	36.41	58.08	51.02	23.08	14.90	23.85	22.85	14.23	13.03	30.38	29.04	17.69	16.09	18.26	18.01	24.23	22.00	28.85	27.05	34.23	33.90								
UGE	43.66	36.10	62.31	59.65	75.38	68.76	29.23	19.97	23.88	22.85	19.23	18.13	21.92	20.81	25.77	24.07	33.91	32.01	34.23	33.03	51.65	50.00	40.84	40.00								
Qwen2.5-VL-3B	36.15	26.01	50.00	47.81	76.15	63.14	25.77	17.08	26.92	25.02	30.77	28.89	44.62	42.79	25.00	22.76	28.70	27.70	26.92	25.12	25.77	25.17	29.62	28.21								
UGE	37.09	29.72	41.54	39.70	65.38	56.67	29.62	21.79	28.08	27.20	24.62	23.02	29.62	28.54	32.31	31.88	29.57	28.30	31.15	30.03	38.85	37.33	38.08	36.89								
Qwen2.5-VL-7B	39.91	30.49	58.85	54.93	76.15	65.19	27.10	18.54	16.15	14.21	9.23	7.03	12.69	10.15	22.31	20.17	26.09	24.11	27.31	27.31	32.69	30.23	35.77	34.17								
UGE	55.87	48.60	70.77	68.58	70.62	59.89	28.08	19.12	22.55	20.90	34.62	33.62	36.15	35.15	48.85	46.46	44.35	43.30	29.23	28.03	58.95	57.71	50.38	49.80								
GME-2B	35.21	20.608	58.85	36.41	64.62	37.54	23.08	12.20	25.00	15.77	17.31	10.92	21.92	13.83	13.46	8.49	25.22	15.91	30.77	19.41	40.00	25.24	37.69	23.78								
UGE	46.01	35.54	55.00	52.30	70.38	67.17	29.23	17.82	16.54	15.47	17.31	15.62	19.62	17.54	12.31	11.85	30.43	29.94	31.54	29.92	38.08	36.15	38.46	<b								

on Singapore; Table 3), reflecting the benefit of aligning spatial graphs with textual and visual representations in UGE. For spatial grounding benchmark, Table 4 shows that UGE consistently improves performance across cities except for Beijing on proximity-based tasks (e.g., nearest POI). This improvement largely stems from the structural encoding of proximity relationships in spatial graphs. In contrast, distance and distance-direction tasks show inconsistent performance. These queries involve fine-grained spatial concepts and explicit relational reasoning—such as directionality, relative orientation, and comparative distance—that may not be fully captured by the multimodal embeddings learned through contrastive training alone. This observation is consistent with prior findings in work on geographic question answering, which show that LLMs and VLMs often struggle with distance, direction, and other fine-grained spatial relations [34, 39, 57].

4.3 Ablation Study

We conduct an ablation study on UGE with the Qwen2.5-VL-7B backbone to assess the impact of key design choices, by selectively modifying the spatial encoder or training curriculum. NoEdgeEncoder removes edge features from the graph encoder. NoPosEncoder removes positional encoding. NodeAttrEncoder removes both edge features and positional encoding, reducing the graph to a node-only representation. STAGE1-ONLY denotes a model fine-tuned using only Stage 1 data, while STAGE2-ONLY is trained directly on Stage 2 data without Stage 1 initialization. As shown in Figure 5, the full model (UGE) generally performs better across four tasks. Removing edge features or positional encoding leads to consistent but moderate degradation. The training curriculum has a larger effect: models trained with only Stage 1 or only Stage 2 data generally underperform the two-stage setup, highlighting the importance of progressively introducing spatial supervision. For metric spatial queries (i.e., distance and distance-direction), NoEdgeEncoder occasionally performs better, suggesting that precisely modeling fine-grained quantitative and directional relations remains nontrivial within current graph-encoded representations. The complete results of the ablation study are included in the Appendix I.

5 Conclusion, Outlook, and Broader Impact

We presented UGE framework for learning spatially grounded multimodal embeddings that aligned street-view images, text, and urban spatial graphs using the UGDATA data pipeline. The proposed two-stage training strategy progressively introduced spatial reasoning cues and graph-conditioned learning to support stable and transferable representations. Evaluations on UGBENCH showed that UGE achieved substantial improvements on various urban tasks across most cities and model backbones. Notably, consistent gains in geolocation ranking and image retrieval suggested that spatial graphs could serve as effective priors for graph-guided geographic information retrieval across modalities. Moreover, our results highlight an important direction for future work: although graph-conditioned embeddings effectively capture relational and contextual spatial cues, improving the representation of fine-grained, metric, and directional spatial information remains essential for stronger spatial understanding and reasoning in multimodal models.

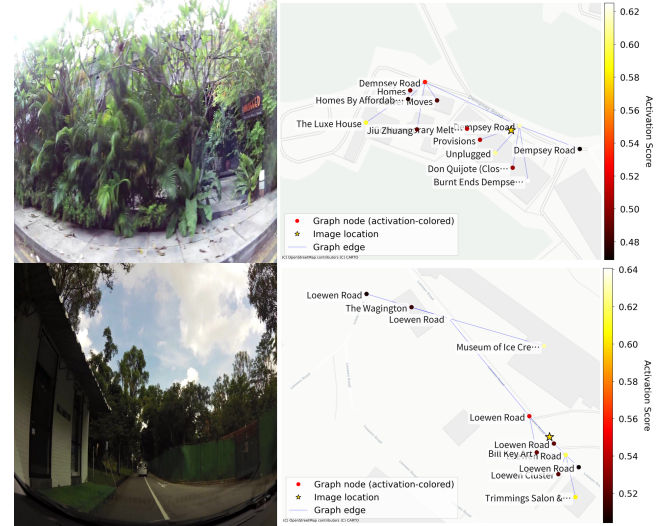


Figure 4: Spatial activation analysis for the depressing perception task. Two Singapore street views with similar greenery show different scores: the lower-depressing case (top) emphasizes activity-related POIs, while the higher-depressing case (bottom) focuses on nearby road segments.

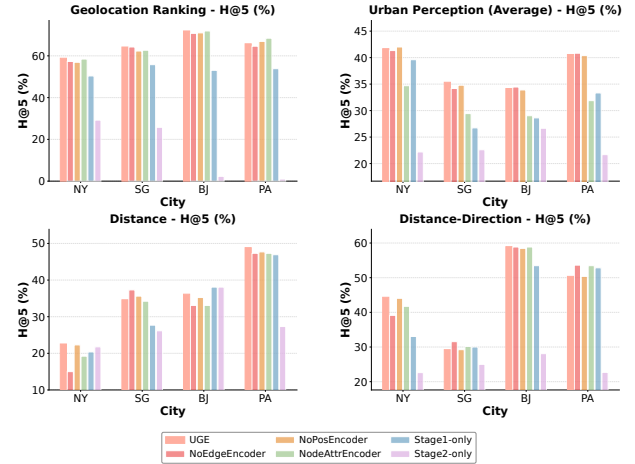


Figure 5: Results of ablation study on Geolocation Ranking, Image Retrieval, Distance, Distance-Direction tasks (Hit@5%).

More broadly, our UGE framework offers a practical foundation for place-centric information retrieval, context-aware image and location search, geographical visual question answering, and AI travel assistants. Given that spatial graphs are easily accessible in real-world settings, we believe this work opens up meaningful directions for integrating explicit spatial context into multimodal models for reliable and interpretable place-centric AI applications.

Acknowledgments

We thank all collaborators for their valuable contributions, insightful discussions, and support throughout this work.

References

- [1] Marah Abdin, Sam Ade Jacobs, Ammar Ahmad Awan, Jyoti Aneja, Ahmed Awadallah, Hany Awadalla, Nguyen Bach, Amit Bahree, Arash Bakhtiari, Jianmin Bao, Harkirat Behl, Alon Benhaim, Misha Bilenko, Johan Björck, Sébastien Bubeck, Qin Cai, Martin Cai, Caio César Teodoro Mendes, Weizhu Chen, Vishrav Chaudhary, Dong Chen, Dongdong Chen, Yen-Chun Chen, Yi-Ling Chen, Parul Chopra, Xiyang Dai, Allie Del Giorno, Gustavo de Rosa, Matthew Dixon, Ronen Eldan, Victor Fragoso, Dan Iter, Mei Gao, Min Gao, Jianfeng Gao, Amit Garg, Abhishek Goswami, Suriya Gunasekar, Emmaan Haider, Junheng Hao, Russell J. Hewett, Jamie Huynh, Mojan Javaheripi, Xin Jin, Piero Kauffmann, Nikos Karampatziakis, Dongwoo Kim, Mahmoud Khademi, Lev Kurilenko, James R. Lee, Yin Tat Lee, Yuanzhu Li, Yunsheng Li, Chen Liang, Lars Liden, Ce Liu, Mengchen Liu, Weishung Liu, Eric Lin, Zeqi Lin, Chong Luo, Piyush Madan, Matt Mazzola, Arindam Mitra, Hardik Modi, Anh Nguyen, Brandon Norick, Barun Patra, Daniel Perez-Becker, Thomas Portet, Reid Pryzant, Heyang Qin, Marko Radmilac, Corby Rosset, Sambuddha Roy, Olatunji Ruwase, Olli Saarikivi, Amin Saied, Adil Salim, Michael Santacroce, Shital Shah, Ning Shang, Hiteshi Sharma, Swadheen Shukla, Xia Song, Masahiro Tanaka, Andrea Tupini, Xin Wang, Lijuan Wang, Chunyu Wang, Yu Wang, Rachel Ward, Guanhua Wang, Philipp Witte, Haiping Wu, Michael Wyatt, Bin Xiao, Can Xu, Jiahang Xu, Weijian Xu, Sonali Yadav, Fan Yang, Jianwei Yang, Ziyi Yang, Yifan Yang, Donghan Yu, Lu Yuan, Chengruidong Zhang, Cyril Zhang, Jianwen Zhang, Li Lyra Zhang, Yi Zhang, Yue Zhang, Yunan Zhang, and Xiren Zhou. 2024. Phi-3 Technical Report: A Highly Capable Language Model Locally on Your Phone. *arXiv preprint arXiv:2404.14219* (2024).
- [2] Shuai Bai, Kegin Chen, Xuejing Liu, Jialin Wang, Wenbin Ge, Sibo Song, Kai Dang, Peng Wang, Shijie Wang, Jun Tang, et al. 2025. Qwen2. 5-vl technical report. *arXiv preprint arXiv:2502.13923* (2025).
- [3] Shaked Brody, Uri Alon, and Eran Yahav. 2021. How attentive are graph attention networks? *arXiv preprint arXiv:2105.14491* (2021).
- [4] Howard Chen, Alane Suhr, Dipendra Misra, Noah Snavely, and Yoav Artzi. 2019. Touchdown: Natural language navigation and spatial reasoning in visual street environments. In *Proceedings of the IEEE/CVF Conference on Computer Vision and Pattern Recognition*. 12538–12547.
- [5] An-Chieh Cheng, Hongxu Yin, Yang Fu, Qushan Guo, Ruihan Yang, Jan Kautz, Xiaolong Wang, and Sifei Liu. 2024. Spatialrgpt: Grounded spatial reasoning in vision-language models. *Advances in Neural Information Processing Systems* 37 (2024), 135062–135093.
- [6] Chen Chu and Cyrus Shahabi. 2025. Geo2Vec: Shape-and Distance-Aware Neural Representation of Geospatial Entities. *arXiv preprint arXiv:2508.19305* (2025).
- [7] Brandon Clark, Alec Kerrigan, Parth Parag Kulkarni, Vicente Vivanco Cepeda, and Mubarak Shah. 2023. Where we are and what we're looking at: Query based worldwide image geo-localization using hierarchies and scenes. In *Proceedings of the IEEE/CVF Conference on Computer Vision and Pattern Recognition*. 23182–23190.
- [8] Marius Cordts, Mohamed Omran, Sebastian Ramos, Timo Rehfeld, Markus Enzweiler, Rodrigo Benenson, Uwe Franke, Stefan Roth, and Bernt Schiele. 2016. The cityscapes dataset for semantic urban scene understanding. In *Proceedings of the IEEE conference on computer vision and pattern recognition*. 3213–3223.
- [9] Marius Cordts, Mohamed Omran, Sebastian Ramos, Timo Scharwächter, Markus Enzweiler, Rodrigo Benenson, Uwe Franke, Stefan Roth, and Bernt Schiele. 2015. The cityscapes dataset. In *CVPR Workshop on the Future of Datasets in Vision*, Vol. 2. 1.
- [10] Angel Daruna, Nicholas Meegan, Han-Pang Chiu, Supun Samarakakera, and Rakesh Kumar. 2025. GeoSURGE: Geo-localization using Semantic Fusion with Hierarchy of Geographic Embeddings. *arXiv preprint arXiv:2510.01448* (2025).
- [11] Nianchen Deng, Lixin Gu, Shenglong Ye, Yinan He, Zhe Chen, Songze Li, Haomin Wang, Xingguang Wei, Tianshuo Yang, Min Dou, et al. 2025. InternSpatial: A Comprehensive Dataset for Spatial Reasoning in Vision-Language Models. *arXiv preprint arXiv:2506.18385* (2025).
- [12] Reid Ewing and Susan Handy. 2009. Measuring the unmeasurable: Urban design qualities related to walkability. *Journal of Urban design* 14, 1 (2009), 65–84.
- [13] Jie Feng, Tianhui Liu, Yuwei Du, Siqi Guo, Yuming Lin, and Yong Li. 2025. Citygpt: Empowering urban spatial cognition of large language models. In *Proceedings of the 31st ACM SIGKDD Conference on Knowledge Discovery and Data Mining* V. 2. 591–602.
- [14] Jie Feng, Shengyuan Wang, Tianhui Liu, Yanxin Xi, and Yong Li. 2025. Urban-LLaVA: A Multi-modal Large Language Model for Urban Intelligence with Spatial Reasoning and Understanding. *arXiv preprint arXiv:2506.23219* (2025).
- [15] Jie Feng, Jun Zhang, Tianhui Liu, Xin Zhang, Tianjian Ouyang, Junbo Yan, Yuwei Du, Siqi Guo, and Yong Li. 2025. Citybench: Evaluating the capabilities of large language models for urban tasks. In *Proceedings of the 31st ACM SIGKDD Conference on Knowledge Discovery and Data Mining* V. 2. 5413–5424.
- [16] Michael Günther, Saba Sturua, Mohammad Kalim Akram, Isabelle Mohr, Andrei Ungureanu, Bo Wang, Sedigheh Eslami, Scott Martens, Maximilian Werk, Nan Wang, et al. 2025. jina-embeddings-v4: Universal embeddings for multimodal multilingual retrieval. In *Proceedings of the 5th Workshop on Multilingual Representation Learning (MRL 2025)*. 531–550.
- [17] Lukas Haas, Michal Skreta, Silas Alberti, and Chelsea Finn. 2024. Pigeon: Predicting image geolocations. In *Proceedings of the IEEE/CVF Conference on Computer Vision and Pattern Recognition*. 12893–12902.
- [18] Xixuan Hao, Wei Chen, Yibo Yan, Siru Zhong, Kun Wang, Qingsong Wen, and Yuxuan Liang. 2025. Urbanlp: Multi-granularity vision-language pretraining for urban socioeconomic indicator prediction. In *Proceedings of the AAAI Conference on Artificial Intelligence*, Vol. 39. 28061–28069.
- [19] James Hays and Alexei A Efros. 2008. Im2gps: estimating geographic information from a single image. In *2008 ieee conference on computer vision and pattern recognition*. IEEE, 1–8.
- [20] Jun He, Yi Lin, Zilong Huang, Jiacong Yin, Junyan Ye, Yuchuan Zhou, Weijia Li, and Xiang Zhang. 2025. Urbanfeel: A comprehensive benchmark for temporal and perceptual understanding of city scenes through human perspective. *arXiv preprint arXiv:2509.22228* (2025).
- [21] Yujun Hou, Matias Quintana, Maxim Khomiakov, Winston Yap, Jiani Ouyang, Koichi Ito, Zeyu Wang, Tianhong Zhao, and Filip Biljecki. 2024. Global Streetscapes—A comprehensive dataset of 10 million street-level images across 688 cities for urban science and analytics. *ISPRS Journal of Photogrammetry and Remote Sensing* 215 (2024), 216–238.
- [22] Lei Hu, Wenwen Li, and Yunqiang Zhu. 2024. Geometric feature enhanced knowledge graph embedding and spatial reasoning. In *Proceedings of the 7th ACM SIGSPATIAL International Workshop on AI for Geographic Knowledge Discovery*. 50–53.
- [23] Qingyong Hu, Bo Yang, Sheikh Khalid, Wen Xiao, Niki Trigoni, and Andrew Markham. 2022. Sensaturban: Learning semantics from urban-scale photogrammetric point clouds. *International Journal of Computer Vision* 130, 2 (2022), 316–343.
- [24] Yufeng Huang, Jiji Tang, Zhuo Chen, Rongsheng Zhang, Xinfeng Zhang, Weijie Chen, Zeng Zhao, Zhou Zhao, Tangjie Lv, Zhipeng Hu, et al. 2024. Structure-clip: Towards scene graph knowledge to enhance multi-modal structured representations. In *Proceedings of the AAAI conference on artificial intelligence*, Vol. 38. 2417–2425.
- [25] Chidubem Iddianozie and Gavin McArdle. 2020. Improved graph neural networks for spatial networks using structure-aware sampling. *ISPRS International Journal of Geo-Information* 9, 11 (2020), 674.
- [26] Filip Ilievski, Pedro Szekely, and Bin Zhang. 2021. Cskg: The commonsense knowledge graph. In *European Semantic Web Conference*. Springer, 680–696.
- [27] Adam Iwniak, Marek Maziarz, and Iwona Kaczmarek. 2023. Spatial analysis in GeoAI with the use of graph neural networks: Quality of life prediction in urban areas case. *Abstracts of the ICA* 6 (2023), 102.
- [28] Ziyuan Jiang, Rui Meng, Xinyi Yang, Semih Yavuz, Yingbo Zhou, and Wenhui Chen. 2024. Vlm2vec: Training vision-language models for massive multimodal embedding tasks. *arXiv preprint arXiv:2410.05160* (2024).
- [29] Konstantin Klemmer, Nathan S Safir, and Daniel B Neill. 2023. Positional encoder graph neural networks for geographic data. In *International conference on artificial intelligence and statistics*. PMLR, 1379–1389.
- [30] Varvara Krechetova and Denis Kochedykov. 2025. Geobenchx: Benchmarking llms for multistep geospatial tasks. *arXiv preprint arXiv:2503.18129* (2025).
- [31] Jaejun Lee, Chanyoung Chung, Hochang Lee, Sungho Jo, and Joyce Whang. 2023. VISTA: Visual-textual knowledge graph representation learning. In *Findings of the association for computational linguistics: EMNLP 2023*. 7314–7328.
- [32] Ween Jiann Lee and Hady W Lauw. 2024. Latent representation learning for geospatial entities. *ACM Transactions on Spatial Algorithms and Systems* 10, 4 (2024), 1–31.
- [33] Feng Li, Renrui Zhang, Hao Zhang, Yuanhan Zhang, Bo Li, Wei Li, Zejun Ma, and Chunyuan Li. 2024. Llava-next-interleave: Tackling multi-image, video, and 3d in large multimodal models. *arXiv preprint arXiv:2407.07895* (2024).
- [34] Yuan-Hong Liao, Rafid Mahmood, Sanja Fidler, and David Acuna. 2024. Reasoning paths with reference objects elicit quantitative spatial reasoning in large vision-language models. *arXiv preprint arXiv:2409.09788* (2024).
- [35] Tianhui Liu, Hetian Pang, Xin Zhang, Jie Feng, Yong Li, and Pan Hui. 2025. CityRISE: Reasoning Urban Socio-Economic Status in Vision-Language Models via Reinforcement Learning. *arXiv preprint arXiv:2510.22282* (2025).
- [36] Linhao Luo, Yuan-Fang Li, Gholamreza Haffari, and Shirui Pan. 2023. Reasoning on graphs: Faithful and interpretable large language model reasoning. *arXiv preprint arXiv:2310.01061* (2023).
- [37] L. Luo, Z. Zhao, C. Gong, G. Haffari, and S. Pan. 2024. Graph-constrained Reasoning: Faithful Reasoning on Knowledge Graphs with Large Language Models. *arXiv* 2024. *arXiv preprint arXiv:2410.13080* (2024).
- [38] Kevin Lynch. 1960. The image of the city/Kevin Lynch. *Social Problems* 8, 3 (1960), 280–281.

- [39] Gengchen Mai, Krzysztof Janowicz, Rui Zhu, Ling Cai, and Ni Lao. 2021. Geographic question answering: challenges, uniqueness, classification, and future directions. *AGILE: GIScience series 2* (2021), 8.
- [40] Timothy P McNamara. 1986. Mental representations of spatial relations. *Cognitive psychology* 18, 1 (1986), 87–121.
- [41] Rui Meng, Ziyang Jiang, Ye Liu, Mingyi Su, Xinyi Yang, Yuepeng Fu, Can Qin, Zeyuan Chen, Ran Xu, Caiming Xiong, et al. 2025. Vlm2vec-v2: Advancing multimodal embedding for videos, images, and visual documents. *arXiv preprint arXiv:2507.04590* (2025).
- [42] Zhiliang Peng, Wenhui Wang, Li Dong, Yaru Hao, Shaohan Huang, Shuming Ma, and Furu Wei. 2023. Kosmos-2: Grounding multimodal large language models to the world. *arXiv preprint arXiv:2306.14824* (2023).
- [43] Sukanya Randhawa, Eren Aygün, Guntaj Randhawa, Benjamin Herfort, Sven Lautenbach, and Alexander Zipf. 2025. Paved or unpaved? a deep learning derived road surface global dataset from mapillary street-view imagery. *ISPRS Journal of Photogrammetry and Remote Sensing* 223 (2025), 362–374.
- [44] Mark Philip Salesse. 2012. *Place Pulse: Measuring the collaborative image of the city*. Ph. D. Dissertation. Massachusetts Institute of Technology.
- [45] Raphael Schumann, Wanrong Zhu, Weixi Feng, Tsu-Jui Fu, Stefan Riezler, and William Yang Wang. 2024. Velma: Verbalization embodiment of llm agents for vision and language navigation in street view. In *Proceedings of the AAAI Conference on Artificial Intelligence*, Vol. 38. 18924–18933.
- [46] Alexander W Siegel and Sheldon H White. 1975. The development of spatial representations of large-scale environments. *Advances in child development and behavior* 10 (1975), 9–55.
- [47] Albert Stevens and Patty Coupe. 1978. Distortions in judged spatial relations. *Cognitive psychology* 10, 4 (1978), 422–437.
- [48] Niket Tandon, Gerard De Melo, Fabian Suchanek, and Gerhard Weikum. 2014. Webchild: Harvesting and organizing commonsense knowledge from the web. In *Proceedings of the 7th ACM international conference on Web search and data mining*. 523–532.
- [49] Junjue Wang, Zhuo Zheng, Ailong Ma, Xiaoyan Lu, and Yanfei Zhong. 2021. LoveDA: A remote sensing land-cover dataset for domain adaptive semantic segmentation. *arXiv preprint arXiv:2110.08733* (2021).
- [50] Peng Wang, Shuai Bai, Sinan Tan, Shijie Wang, Zhihao Fan, Jinze Bai, Keqin Chen, Xuejing Liu, Jialin Wang, Wenbin Ge, et al. 2024. Qwen2-vl: Enhancing vision-language model's perception of the world at any resolution. *arXiv preprint arXiv:2409.12191* (2024).
- [51] Azmine Toushik Wasi, Wahid Faisal, Abdur Rahman, Mahfuz Ahmed Anik, Munem Shahriar, Mohsin Mahmud Topu, Sadia Tasnim Meem, Rahatun Nesa Priti, Sabrina Afroz Mitu, Md Iqrarul Hoque, et al. 2026. SpatialLab: Can Vision-Language Models Perform Spatial Reasoning in the Wild? *arXiv preprint arXiv:2602.03916* (2026).
- [52] Meiliu Wu and Qunyong Huang. 2022. Im2city: image geo-localization via multi-modal learning. In *Proceedings of the 5th ACM SIGSPATIAL International Workshop on AI for Geographic Knowledge Discovery*. 50–61.
- [53] Haotian Xu, Yue Hu, Chen Gao, Zhengqiu Zhu, Yong Zhao, Yong Li, and Quanjun Yin. 2025. Geonav: Empowering llmns with explicit geospatial reasoning abilities for language-goal aerial navigation. *arXiv preprint arXiv:2504.09587* (2025).
- [54] Haotian Xu, Yue Hu, Zhengqiu Zhu, Chen Gao, Ziyou Wang, Junreng Rao, Wen-hao Lu, Weishi Li, Quanjun Yin, and Yong Li. 2026. CityCube: Benchmarking Cross-view Spatial Reasoning on Vision-Language Models in Urban Environments. *arXiv preprint arXiv:2601.14339* (2026).
- [55] Weihao Xuan, Junjue Wang, Heli Qi, Zihang Chen, Zhuo Zheng, Yanfei Zhong, Junshi Xia, and Naoto Yokoya. 2025. DynamicVL: Benchmarking Multimodal Large Language Models for Dynamic City Understanding. *arXiv preprint arXiv:2505.21076* (2025).
- [56] Gevorg Yeghikyan, Felix L Opalka, Mirco Nanni, Bruno Lepri, and Pietro Lio. 2020. Learning mobility flows from urban features with spatial interaction models and neural networks. In *2020 IEEE international conference on smart computing (SMARTCOMP)*. IEEE, 57–64.
- [57] Sahiti Yerramilli, Nilay Pande, Rynaa Grover, and Jayant Sravan Tamarapalli. 2025. GeoChain: Multimodal Chain-of-Thought for Geographic Reasoning. *arXiv preprint arXiv:2506.00785* (2025).
- [58] Dazhou Yu, Riyang Bao, Gengchen Mai, and Liang Zhao. 2025. Spatial-rag: Spatial retrieval augmented generation for real-world spatial reasoning questions. *arXiv preprint arXiv:2502.18470* (2025).
- [59] Weichen Zhang, Chen Gao, Shiquan Yu, Ruiying Peng, Baining Zhao, Qian Zhang, Jinqiang Cui, Xinlei Chen, and Yong Li. 2025. CityNavAgent: Aerial Vision-and-Language Navigation with Hierarchical Semantic Planning and Global Memory. *arXiv preprint arXiv:2505.05622* (2025).
- [60] Xin Zhang, Yanzhao Zhang, Wen Xie, Mingxin Li, Ziqi Dai, Dingkun Long, Pengjun Xie, Meishan Zhang, Wenjie Li, and Min Zhang. 2024. GME: Improving Universal Multimodal Retrieval by Multimodal LLMs. *arXiv preprint arXiv:2412.16855* (2024).

Appendices

A Training Data Samples

A.1 Stage 1: Instruction-Guided Image-Text Alignment.

Type 1: Image with Spatial Reasoning Path (SRP). This type injects spatial knowledge through language by pairing an image with a spatial reasoning path expressed in text.

```
{
  "messages": [
    {
      "role": "user",
      "content": "<image> Describe if this viewpoint is reachable or the destination is reachable from the viewpoint."
    }
  ],
  "positive_messages": [
    {
      "role": "user",
      "content": "... Spatial Reasoning Path: (539125490832143, nearest, Kallang Road) (2.0m, 342°(N)) -> (3.2m, 72°(E)) -> (Kallang Road, Intersection of Geylang Road and Kallang Road) -> (375.8m, 206°(SW)) -> (Geylang Road, near, Kallang Riverside Park North) -> (Kallang Riverside Park North, bounds, Kampong Bugis) -> (193.5m, 263°(W)) -> (Kampong Bugis, near, Banyan Tree & Ruin) (28.4m, 114°(SE)). Based on the spatial context, you can reach Banyan Tree & Ruin from the current image location at (103.8693, 1.3100)."
    }
  ],
  "label": 1,
  "images": [".../singapore/images/539125490832143.jpg"],
  "graphs": [],
  "pair_type": "stage1_image_only"
}
```

Type 2: Image-Level Captioning. This type aligns images with detailed semantic descriptions without explicit graph input.

```
{
  "messages": [
    {
      "role": "user",
      "content": "<image> Provide detailed descriptions of the image content."
    }
  ],
  "positive_messages": [
    {
      "role": "user",
      "content": "The image captures a sunlit urban street scene on Broadway in Harlem, New York City, near the intersection of West 147th Street..."
    }
  ],
  "label": 1,
  "images": [".../newyork/images/2936878419934510.jpg"],
  "graphs": [],
  "pair_type": "stage1_image_only"
}
```

A.1 Stage 2: Graph-Conditioned Spatial Embedding.

Type 1: Image-Graph with Spatial Reasoning Path. This type conditions learning on both the local spatial graph and an explicit spatial reasoning path, providing distance-direction cues and grounded place entities.

```
{
  "messages": [
    {
      "role": "user",
      "content": "<graph><image> Note on path notation: Triple indicates the decision point information in the path, the arrow '→' indicates the next step in the path, and parentheses (e.g., (50m, S)) immediately after a triple describe the distance and direction from the source to the target node. Based on the spatial context represented in graph and the spatial reasoning path, you can reach Ps 234 from the current location shown in the image with id 1360629940984808 at (-73.9196, 40.7724). Here are relevant place entities informations: {'1360629940984808': {'id': '1360629940984808', 'category': 'mapillary', 'coordinates': 'POINT(lon: -73.91961277, lat: 40.77240744)'}, '27 St': {'id': '538146', 'category': 'None', 'coordinates': 'LINE(...)'}, '20 Ave': {'id': '537435', 'category': 'None', 'coordinates': 'LINE(...)'}, 'Ps 234': {'id': '568292', 'category': 'None', 'coordinates': 'POINT(lon: -73.92307984, lat: 40.76702346)'}, ... }",
      "content": "You can reach Ps 234 from the current location shown in the image with id 1360629940984808 at (-73.9196, 40.7724)."
    }
  ],
  "images": ".../newyork/images/1360629940984808.jpg",
  "graphs": [
    ".../subgraphs/subgraph_1360629940984808.pkl"
  ],
  "summarization": "You can reach Ps 234 from the current location shown in the image with id 1360629940984808 at (-73.9196, 40.7724).",
  "image_coordinates": "(-73.9196, 40.7724)",
  "mapillary_node": "1360629940984808"
}
```

Type 2: Image-Graph Spatial Context Description. This type fuses visual content and the local spatial graph to produce a holistic description of the scene and its surrounding urban context.

```
{
  "messages": [
    {
      "role": "user",
      "content": "<graph><image> Use the image and graph together to describe the scene and its spatial context."
    }
  ],
  "positive_messages": [
    ...
  ]
}
```

```

[{"role": "user",
 "content": "This image aligns closely with the spatial context of Bukit Batok, a planned residential town in West District in Singapore. The location corresponds to a node near the complex crossing of Bukit Batok East Avenue 6 and Bukit Batok East Avenue 3..."}
],
{"label": 1,
 "images": [
 ".../singapore/images/1526294631371000.jpg"
 ],
 "graphs": [
 ".../subgraphs/mapillary_1526294631371000_subgraph.pkl"
 ],
 "pair_type": "stage2_fusion"
}
]

```

B Prompt for Spatial Context Caption Generation

To generate spatial context captions, we use a structured prompt that conditions image captioning on a localized urban spatial graph. The prompt consists of fixed instructions and a dynamic component, denoted as `{subgraph_desc}`, which describes the spatial subgraph surrounding each street-view image.

Prompt Overview. The model is instructed to generate detailed captions for urban street images given a comprehensive spatial network context. The spatial context is provided as a textual description of a localized spatial graph derived from OpenStreetMap data.

Caption Generation Instructions. Given a single street-view image within the spatial network described above, the model is asked to produce:

- **Detailed Image Caption**, describing image-specific visual features, including: locations, architectural characteristics, businesses and landmarks, vegetation and natural elements, visual indicators of acoustic environments (e.g., traffic or quiet settings), cues related to odors (e.g., vegetation, cafes, exhaust), and colors, materials, or textures influencing thermal and psychological perception.

- **Summarization of Image Features within Spatial Context**, focusing on visual elements that reflect or situate the image within its broader urban environment, such as neighborhood identity, street structure, proximity to other locations, characteristic urban design patterns, street signs or landmarks, and overall multi-sensory qualities affecting psychological well-being.

Additional Guidelines. The model is instructed to explicitly relate visual observations to entities and locations described in the spatial network, and to consider the interaction between visual, acoustic, and olfactory cues when characterizing the urban environment.

Spatial Context Caption Prompt. We use the following prompt to generate spatial context captions for each street-view image. The prompt conditions caption generation on a localized urban spatial graph description. The only dynamic component is `{subgraph_desc}`, which is generated per image.

```

You are an advanced vision model tasked with generating detailed captions for urban street images within a comprehensive spatial network context.

# Comprehensive Spatial Context:
## Network Structure:
{subgraph_desc}

# Enhanced Caption Generation Instructions:
You will be provided with one street image from the spatial area described in the Network Structure above. The image is situated within a spatial context represented by graph information.

For the image, generate a detailed caption and then summarize the image features based on the spatial context.

1. Detailed image caption:
Describe the unique visual features of the image, including:
- Locations
- Distinctive architectural features
- Notable businesses, signage, or landmarks
- Vegetation, greenery, water features, or natural elements
- Visual indicators of acoustic environments (traffic, construction, quiet settings)
- Elements suggesting odors (vegetation, cafes, trash bins, traffic exhaust)
- Colors, materials, and textures influencing thermal and psychological perception

2. Summarization of image features within spatial context:
Focus on visual elements that reflect spatial context, including:
- Clues indicating the neighborhood or area
- Street features aligned with the network (crossings, width, type)
- Visual indicators of proximity to other locations in the network
- Architectural or urban design elements characteristic of the region
- Street signs, direction indicators, or landmarks situating the image
- Overall multi-sensory quality influencing psychological wellbeing

# Output Format:
Image:
<caption>

Summarization:
<summary>

# Instructions:
- Prefix captions with "Image:"
- End with a "Summarization:" section
- Connect visual observations to spatial connectivity patterns
- Refer to locations and entities in the network description
- Consider interactions of visual, acoustic, and olfactory cues

```

C Construction of Subgraph Description

To generate spatial context captions, we condition image captioning on a localized urban spatial graph. The prompt consists of fixed instructions and a dynamic component, denoted as `{subgraph_desc}`, which encodes the spatial structure surrounding each street-view image.

Dynamic Subgraph Description (`{subgraph_desc}`). The subgraph description is generated by the function

`_create_network_description()` and is unique to each image. It reflects a localized OpenStreetMap-derived spatial graph centered at the image location. While the description follows a fixed structural template, its content (nodes, edges, attributes, distances, and directions) varies depending on the extracted subgraph.

Structure of the Subgraph Description. Each subgraph description is composed of four main sections:

- **Network Overview.** A header summarizing the graph size, formatted as: *“This network contains N locations, with C center nodes and E connections.”*
- **Center Nodes.** One or more nodes corresponding to the image location(s) in the graph. Each center node is described by its identifier, semantic type, geometry, available attributes, geographic coordinates, and relative orientation.
- **Nearby Locations.** Up to ten nodes that are directly connected to the center node or lie within approximately 200 meters. These locations are sorted by distance and described using their name (if available), identifier, type, geometry, attributes, coordinates, and relative direction.
- **Locations Connected to Nearby Areas.** One-hop neighbors of the nearby locations, with up to twelve entries. These nodes follow the same descriptive format and provide extended neighborhood context.
- **Connections in the Network.** Explicit descriptions of edges, including: (i) connections between image locations and nearby areas, and (ii) connections among nearby areas. Each edge is annotated with relationship type (e.g., nearest, crossing, intersection), relative direction, distance, and crossing coordinates when applicable.

Node and Edge Attributes. Node descriptions may include attributes such as building use, historic district, architect, building type, address information (street, housenumber, postcode), planning area, district, city, and country. Edge descriptions include relationship type, bearing or direction, distance, and crossing identifiers or coordinates when available.

Example Subgraph Description. For illustration, a subgraph description may state that the image location lies near Orchard Road, ION Orchard, and Somerset MRT, and describe their relative distances, directions, and interconnections. In practice, the exact wording and attribute sets depend on the outputs of

`_extract_node_info()`, `_get_edge_relationship_description()`, and the available fields in the extracted node and edge GeoDataFrames.

Usage in Caption Generation. The generated `{subgraph_desc}` is inserted into the spatial context prompt and provided alongside the image. This enables the model to generate captions and summaries that explicitly relate visual observations to surrounding

streets, landmarks, connectivity patterns, and neighborhood structure, grounding image semantics within the broader urban spatial context.

D Spatial Reasoning Path Generation

For spatial grounding and navigation-style supervision, we generate *Spatial Reasoning Paths* (SRPs) that describe plausible routes from a street-view image location to destination nodes in the surrounding urban spatial graph. These paths are used as an additional dynamic component in spatial reasoning prompts.

Path Generation Pipeline. Each spatial reasoning path is generated through a multi-stage pipeline consisting of path discovery, filtering, formatting, and prompt integration.

- **Path Discovery.** Starting from the image location (Mapillary node), we enumerate candidate paths to diverse destination nodes in the spatial graph using a breadth-first search over a precomputed adjacency structure.
- **Path Filtering and Selection.** Candidate paths are filtered based on hop distance, geometric distance thresholds, and node types (e.g., excluding trivial intersections). To encourage diversity, paths of varying lengths are sampled across different hop distances.
- **Path Formatting.** Selected paths are converted into structured textual representations consisting of relation triples and distance–direction annotations, producing a compact and interpretable spatial reasoning path.
- **Training Data Integration.** The formatted spatial reasoning path is inserted into the user prompt as a dedicated *Spatial Reasoning Path* section, together with a brief explanation of the path notation.

Path Discovery Strategy. Destination nodes are categorized by geometric type, including polygonal entities (e.g., buildings or areas), linear entities (e.g., streets and roads), and point entities (e.g., landmarks or intersections). A reverse breadth-first search from the image location identifies reachable nodes within a maximum hop limit. Candidates are prioritized by geometric distance from the image location, with fallback to more distant nodes when necessary. For each selected destination, the shortest valid path satisfying minimum hop constraints is constructed.

Path Notation and Format. Each spatial reasoning path is expressed using a structured notation composed of relation triples and distance–direction tuples. Triples encode decision points along the route, while arrows indicate progression between successive steps.

- **Triples.** Each triple has the form `(source, relation, target)`, where source and target correspond to named OSM entities (e.g., streets, intersections, or landmarks). Relation types include street names, nearest, near, bounds, intersects, intersection, and complex_crossing.
- **Distance–Direction Tuples.** Each tuple specifies the distance (in meters) and bearing (in degrees with cardinal direction) between connected entities. Tuples may appear immediately after a triple or between steps to describe transitions along the path.

- **Arrow Separators.** The symbol \rightarrow denotes progression to the next step in the route.

Illustrative Example. An example spatial reasoning path may begin at an intersection, move along a street segment for several hundred meters in a given direction, pass through a complex crossing, and terminate near a destination landmark. Such paths explicitly expose relative distance, directionality, and connectivity, enabling navigation-style spatial reasoning grounded in the underlying urban graph.

Role in Training and Evaluation. By translating graph-structured spatial relationships into compact linguistic paths, SRPs provide a bridge between urban spatial graphs and language-based supervision. They enable models to learn spatial concepts such as proximity, direction, and multi-hop connectivity in a form compatible with instruction-guided multimodal embedding learning.

E Benchmark Task Samples

We provide representative examples from the four benchmark tasks used to evaluate spatially grounded urban embeddings.

E.5 Geolocation Ranking. This task evaluates fine-grained location discrimination by ranking candidate textual location descriptions given a street-view image.

```
{
  "messages": [
    {
      "role": "user",
      "content": "<image> Where is this street view image taken?  
Select the correct location:"
    }
  ],
  "images": [.../newyork/images/387138539252309.jpg"],
  "graphs": null,
  "ground_truth": "on Queens Blvd, near Intersection of 32 Pl and Queens Blvd, close to Sunnyside, in Sunnyside, Queens",
  "candidates": [
    "on Queens Blvd, near Intersection of 32 Pl and Queens Blvd, close to Sunnyside, in Sunnyside, Queens",
    "on Queens Blvd, near Intersection of 39 St and Queens Blvd, close to Sunnyside, in Sunnyside, Queens",
    "on Queens Plz S, near Intersection of Connector and Queens Plz, close to Long Island City, Queens",
    "... (remaining candidates omitted)"
  ]
}
```

E.5 Image Retrieval with Spatial Graph Context. This task evaluates text-graph-image alignment by retrieving the correct image given a spatial graph and textual spatial description.

```
{
  "messages": [
    {
      "role": "user",
      "content": "<graph> With reference to the spatial graph, pick the image captured near the intersection of 3rd Avenue and East 10th Street in Manhattan."
    }
  ],
  "images": [],
  "graphs": [.../subgraphs/mapillary_497894054880543_subgraph.pkl],
  "candidate_images": [
    ".../images/526798132036513.jpg",
    ".../images/2609168706058382.jpg",
    ".../images/497894054880543.jpg",
  ]
}
```

```
    "... (remaining candidates omitted)"
  ],
  "ground_truth_idx": 12,
  "ground_truth": ".../images/497894054880543.jpg"
}
```

E.5 Urban Perception Prediction (Depressiveness). This task evaluates high-level urban perception by ranking discretized perception labels derived from human annotations.

```
{
  "messages": [
    {
      "role": "user",
      "content": "<image> What is the perception of depressing for this urban location?"
    }
  ],
  "images": [.../beijing_paris_tokyo/285075470021284.jpg],
  "graphs": [],
  "ground_truth": "Less depressing, Depressing Score: 4.5",
  "candidates": [
    "Not depressing, Depressing Score: 2.5",
    "Less depressing, Depressing Score: 4.5",
    "Moderately depressing, Depressing Score: 6.0",
    "Very depressing, Depressing Score: 9.0",
    "... (remaining candidates omitted)"
  ]
}
```

E.5 Spatial Grounding: Distance Query. This task evaluates metric spatial reasoning by predicting distances between entities using both image and graph context.

```
{
  "messages": [
    {
      "role": "user",
      "content": "<image><graph> How far is the nearest finance from the closest amenity?"
    }
  ],
  "images": [.../paris/images/4321631924514461.jpg],
  "graphs": [.../paris/subgraphs/subgraph_4321631924514461.pkl],
  "ground_truth": "33 meters",
  "candidates": [
    "33 meters",
    "101 meters",
    "304 meters",
    "506 meters",
    "800 meters",
    "1206 meters"
  ]
}
```

F Details of Finetuning UGE

Stage 1 training uses batch sizes in {8, 9, 10, 12} for image–text contrastive learning, while Stage 2 adopts smaller batch sizes {3, 4} to accommodate graph-conditioned inputs. The graph encoder uses two GNN layers with edge-aware attention, 64-dimensional edge encoding and spatial positional encoding [32], producing node embeddings projected to the VLM hidden dimension. To ensure stable training when introducing the graph modality, we apply differentiated learning rates, updating the graph encoder at 5×10^{-5} while scaling VLM parameter updates to 10% of this rate. We use different hardware configurations across training stages and model

families. Stage 2 fine-tuning of the LLaVA1.6-Mistral uses 4 NVIDIA A800 GPUs for 3 epochs (≈ 1 day and 12 hours), while all other models are trained on 4 NVIDIA RTX 5000 GPUs for 5 epochs (12–18 hours).

G Results of Each Task in Urban Perception Benchmark

Table 5 and Table 6 presents per-task results for the urban perception benchmark which show inconsistent performance across different attributes of urban perceptions.

H Results of Nearest Street Task in Spatial Grounding Benchmark

Table 7 presents per-city results for the *Nearest Street* task in the spatial grounding benchmark. Generally, UGE models perform better than the baselines, especially in training cities.

Table 7: Results of Nearest Street task (H@5 / N@5, %).

Model	NY		SG		BJ		PA	
	H@5	N@5	H@5	N@5	H@5	N@5	H@5	N@5
Qwen2-VL-2B	40.29	25.15	27.83	15.84	18.17	10.98	20.00	11.78
UGE	42.09	28.68	49.83	31.63	32.83	20.45	39.67	26.76
Qwen2-VL-7B	34.17	19.62	25.33	14.35	10.33	7.55	56.33	34.91
UGE	44.60	32.43	55.00	37.19	51.00	30.41	49.00	32.94
Qwen2.5-VL-3B	25.54	14.71	23.00	13.67	39.33	29.37	34.17	21.67
UGE	37.41	23.40	33.67	19.57	50.67	33.87	49.83	31.93
Qwen2.5-VL-7B	37.41	22.59	30.50	15.88	25.00	19.02	20.00	12.19
UGE	38.13	26.18	55.17	37.71	41.90	32.04	52.20	34.30
GME-2B	36.69	18.74	29.83	14.55	48.67	23.90	27.33	13.45
UGE	40.29	24.78	45.67	29.29	22.33	11.25	48.17	28.77
VLM2VEC-2B	24.10	13.03	22.50	12.50	23.17	15.30	8.17	4.20
UGE	40.65	27.40	53.83	35.41	28.00	17.05	34.83	23.38
LLaVA1.6	22.66	12.98	21.83	12.35	53.83	31.96	30.17	16.21
UGE	47.84	34.91	69.33	46.82	33.83	20.56	45.00	31.29
Phi3-V	25.54	15.10	25.17	14.04	36.33	20.77	34.00	20.29
UGE	40.29	28.03	48.17	31.99	32.50	17.71	45.50	29.18

I Additional Ablation Studies

This section presents ablation results that disentangle the contributions of individual components in our two-stage training pipeline across geolocation ranking, image retrieval, urban perception, and spatial grounding tasks. For geolocation ranking, Figure 6 shows that the full model (UGE) generally outperforms its variants, indicating that both the complete spatial encoder and the two-stage training curriculum contribute to more discriminative embeddings for location detection. Figure 7 reveals that although UGE generally performs better in terms of Hit@5, fine-tuning using only Stage 1 data outperforms other model variants in ranking quality, especially in held-out cities. Figure 8 evaluates high-level urban perception, reporting average performance across perceptual attributes and shows that UGE yield the best overall performance. Figures 9 and 10 show that variants removing edge features or positional encodings (NoEDGEENCODER, NoPosENCODER, NODEATTRENCODER) exhibit moderate yet systematic performance degradation. In contrast,

models trained without the two-stage curriculum (STAGE1-ONLY, STAGE2-ONLY) display more inconsistent gains across different city contexts. This suggests that the alignment introduced in Stage 1 already enables the VLM embeddings to capture certain proximity-related spatial cues, even without explicit graph-conditioned supervision. Figures 11 and 12 present ablation results on distance-aware and compositional spatial queries. Across model variants, performance gains are less consistent than in proximity-based tasks. Variants without edge encoding occasionally outperform the full model on these metric queries, reflecting the challenge of encoding precise quantitative and directional relations within the current graph-based embedding framework. These results further highlight the limits of existing spatial representations for metric reasoning, despite their effectiveness for proximity-based grounding.

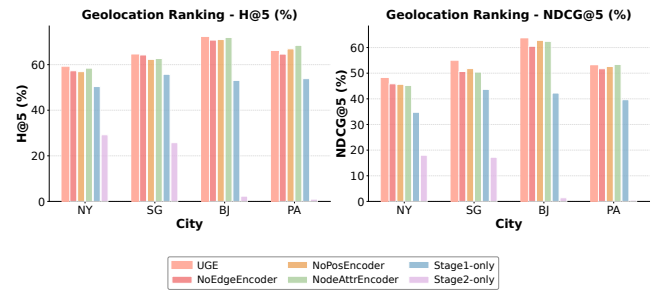


Figure 6: Results of ablation study on Geolocation Ranking.

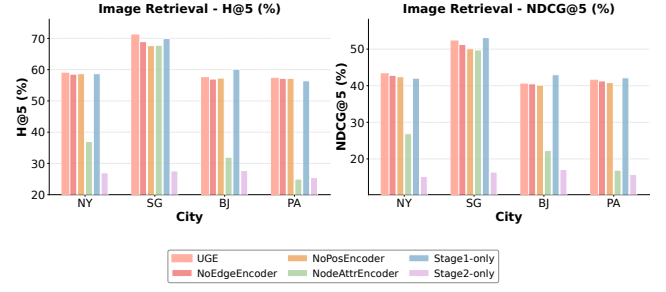


Figure 7: Results of ablation study on Image Retrieval.

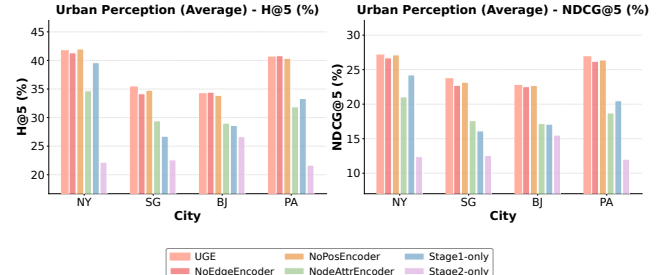


Figure 8: Average results of ablation study on Urban Perception.

Table 5: Urban perception results on *Safe*, *Wealthy*, and *Lively* (H@5 / N@5, %).

Model	Safe								Wealthy								Lively																																
	NY				SG				BJ				PA				NY				SG				BJ				PA																				
	Hit	NDCG	Hit	NDCG	Hit	NDCG	Hit	NDCG	Hit	NDCG	Hit	NDCG	Hit	NDCG	Hit	NDCG	Hit	NDCG	Hit	NDCG	Hit	NDCG	Hit	NDCG	Hit	NDCG	Hit	NDCG																					
Qwen2-VL-2B	32.90	20.00	35.99	21.93	45.24	26.44	42.93	24.91	30.59	16.41	21.34	11.72	26.99	15.63	31.11	20.46	11.05	6.66	17.99	10.94	15.42	8.51	5.66	3.44	UGE	33.16	20.40	36.76	22.98	48.84	28.33	43.44	25.61	32.90	17.83	31.88	19.33	24.42	12.83	20.11	15.75	31.11	18.75	18.61	11.42	12.80	6.95	31.62	17.84
	24.68	12.75	26.99	15.41	40.62	21.39	29.05	15.99	34.96	20.08	30.33	17.78	32.39	19.11	26.22	15.47	31.11	16.61	31.62	18.29	17.99	10.69	20.05	12.07																									
Qwen2-VL-7B	19.02	10.74	17.22	11.08	36.25	24.20	25.71	13.31	13.62	6.27	24.42	12.90	27.25	16.62	20.05	10.34	27.51	14.93	19.79	9.05	19.56	15.85	33.68	18.44	UGE	27.51	15.30	25.45	17.02	16.20	11.00	20.05	13.22	32.13	18.12	43.19	25.68	33.93	20.56	39.07	21.28	20.33	12.08	30.33	17.90	32.90	22.55	37.02	21.25
	37.02	25.30	31.11	20.83	36.76	24.09	31.36	20.03	35.48	22.26	40.87	28.87	35.28	23.80	45.50	21.31	60.93	42.40	39.85	26.77	37.08	24.23	48.59	33.56		UGE	26.22	12.56	29.82	15.06	37.02	17.60	27.51	13.17	25.45	12.17	29.31	14.86	21.59	10.55	14.14	6.73	23.19	14.33	23.39	11.67	19.28	9.58	24.68
GME-2B	33.23	17.41	39.07	23.75	22.62	13.48	24.16	13.23	22.37	12.60	33.68	21.13	26.99	17.50	21.59	12.33	9.51	4.35	7.97	4.69	13.11	6.83	11.83	6.72	UGE	41.39	23.55	17.99	10.81	38.82	22.66	29.05	16.62	22.11	12.94	17.91	9.13	20.57	10.84	15.17	8.78	37.28	21.74	25.71	14.93	11.31	7.46	19.03	10.41
	35.73	23.84	27.25	16.05	28.79	17.92	25.45	14.64	29.07	16.89	36.50	20.72	32.39	18.88	21.08	11.92	56.82	33.77	33.68	21.89	37.53	21.81	53.98	28.89		35.90	23.98	21.85	11.81	19.79	11.23	20.31	11.75	32.65	18.90	27.51	17.19	24.16	14.29	17.48	9.84	62.99	39.25	34.70	20.93	36.50	22.59	40.87	24.63
Phi3-V	31.36	17.63	30.34	17.18	26.48	13.79	24.68	13.90	31.11	18.35	41.65	24.94	29.84	25.74	15.79	28.02	15.98	38.05	19.72	39.07	23.64	37.79	21.83	41.90	23.30	UGE	36.51	20.25	30.85	18.53	43.70	25.85	35.99	21.80	26.99	15.26	30.59	17.83	29.05	18.18	30.85	18.23	21.85	12.17	22.37	13.45	23.91	14.38	

Table 6: Urban perception results on *Depressing*, *Beautiful*, and *Boring* (H@5 / N@5, %).

Model	Depressing												Beautiful												Boring																								
	NY				SG				PA				NY				SG				BJ				PA				NY				SG				BJ				PA								
	Hit	NDCG	Hit	NDCG	Hit	NDCG	Hit	NDCG	Hit	NDCG	Hit	NDCG	Hit	NDCG	Hit	NDCG	Hit	NDCG	Hit	NDCG	Hit	NDCG	Hit	NDCG	Hit	NDCG	Hit	NDCG	Hit	NDCG	Hit	NDCG	Hit	NDCG	Hit	NDCG	Hit	NDCG	Hit	NDCG									
Qwen2-VL-2B	7.46	3.30	12.34	6.60	15.98	8.09	15.68	8.09	41.39	23.47	27.74	17.18	21.85	11.40	35.73	23.80	13.11	8.72	11.83	6.66	15.71	9.76	13.37	8.38	UGE	36.25	21.08	14.40	8.56	11.57	6.58	20.82	12.34	36.50	21.28	34.29	21.65	31.88	18.11	20.06	11.50	18.87	12.26	25.96	14.00	13.88	8.37	22.37	13.46
Qwen2-VL-7B	12.34	5.40	28.53	14.68	44.99	29.10	18.51	7.79	16.20	7.70	29.05	19.05	10.03	5.10	22.37	12.51	12.08	5.64	26.99	14.83	26.22	14.76	14.40	6.59	UGE	43.96	26.61	37.79	22.93	19.28	10.52	32.13	19.50	25.96	15.25	24.42	14.58	27.76	16.25	25.45	15.63	31.11	16.82	25.96	15.83	16.45	9.09	34.45	18.68
Qwen2.5-VL-3B	14.50	12.27	11.57	6.26	14.65	7.94	9.00	4.77	30.59	17.94	31.36	18.48	11.57	8.21	28.02	16.55	24.42	12.83	11.57	7.26	6.94	3.51	6.68	4.06	UGE	15.17	11.09	12.85	5.85	11.05	5.38	12.85	6.74	32.39	18.33	26.99	15.60	24.16	15.22	35.48	20.57	25.36	13.58	18.25	11.47	10.28	7.04	14.40	9.60
Qwen2.5-VL-7B	17.48	7.18	25.96	13.50	35.99	22.54	19.79	10.33	27.51	15.34	29.31	15.60	23.39	15.07	28.79	17.02	4.63	2.51	7.20	4.56	7.46	4.08	6.17	3.35	UGE	50.13	33.53	46.02	31.95	47.56	33.11	50.90	36.22	35.22	21.25	32.13	19.81	28.79	18.60	28.89	17.12	31.36	17.98	22.11	13.86	19.54	12.42	38.30	22.81
GME-2B	33.16	16.83	34.45	16.59	30.85	15.08	33.16	16.43	25.45	12.44	21.08	9.86	22.11	10.40	21.08	10.45	34.70	17.23	31.36	15.07	49.36	24.58	38.82	18.87	UGE	33.23	17.41	39.07	23.75	22.62	13.48	21.46	13.23	22.37	12.60	33.68	21.13	26.99	17.50	21.59	12.33	29.51	14.35	27.97	10.69	13.11	6.83	11.83	6.72
VLM2VEC-2B	21.85	10.10	23.65	10.83	19.79	9.17	21.34	10.09	20.05	10.14	32.90	16.74	19.28	9.25	21.59	10.63	32.73	17.34	23.65	10.30	35.73	17.34	39.59	19.43	UGE	28.28	14.10	29.31	16.71	20.31	11.84	26.74	15.38	33.93	20.99	34.96	22.24	29.82	18.55	31.36	18.14	23.14	12.04	26.74	15.48	25.74	10.63	29.05	15.92
Llava 1.7	15.68	7.07	15.68	8.84	17.22	10.81	16.71	9.64	31.11	19.45	19.54	10.78	25.45	15.46	23.65	13.59	5.66	3.98	7.71	4.84	6.43	3.64	6.43	3.79	UGE	25.68	12.73	17.79	9.53	17.74	10.32	19.79	10.02	24.42	14.24	28.53	16.90	15.94	9.34	24.88	14.66	31.62	18.06	16.71	8.93	25.96	15.67	23.14	11.53
Phi3-V	6.17	2.64	18.25	8.69	14.65	6.95	10.28	5.54	38.82	23.09	37.02	21.91	23.39	15.02	34.45	20.28	17.48	8.80	24.42	12.93	13.88	7.25	16.45	9.37	UGE	38.56	24.41	23.65	13.74	22.62	14.42	29.05	17.85	29.56	14.91	26.74	16.65	26.99	14.30	17.85	9.72	17.74	9.84	21.59	11.38	19.28	9.89		

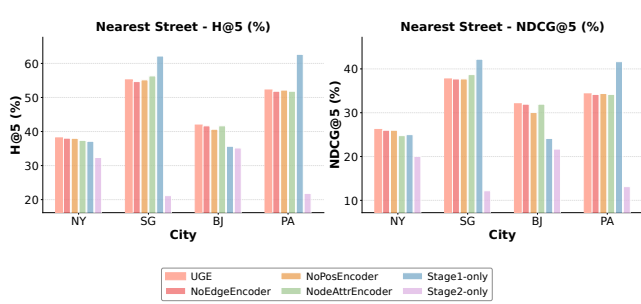


Figure 9: Results of ablation study on *Nearest Street*.

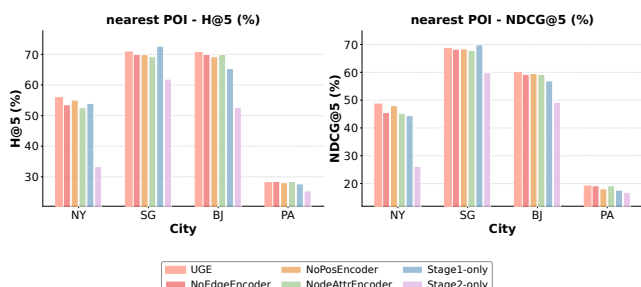


Figure 10: Results of ablation study on *Nearest POI*.

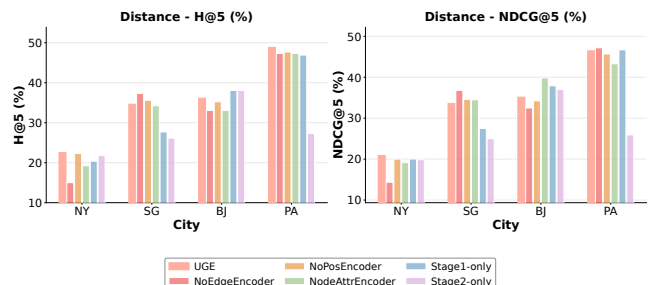


Figure 11: Results of ablation study on *Distance*.

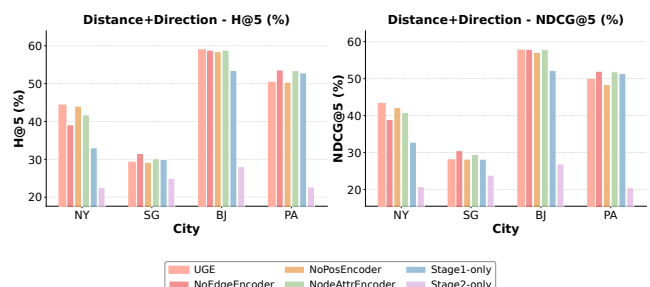


Figure 12: Results of ablation study on *Distance-Direction*.

J Hyperparameter Study

We study two key hyperparameters: the edge embedding dimension of the graph encoder and the learning-rate ratio between the Stage-2 graph encoder and LoRA adapters. As shown in Figure 13, an edge embedding dimension of 64 consistently yields the best performance. Figure 14 further shows that controlling updates to the image–text alignment is critical for stable spatial knowledge injection, with smaller learning-rate ratios generally improving representation quality, while image retrieval benefits from stronger joint learning among graph, image, and text.

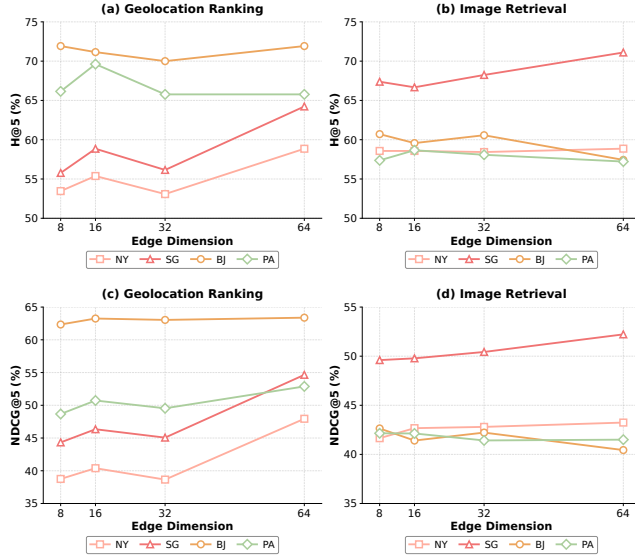


Figure 13: Effect of edge embedding dimension in the graph encoder. (a,b) Hit@5 on geolocation ranking and image retrieval. (c,d) NDCG@5 on geolocation ranking and image retrieval.

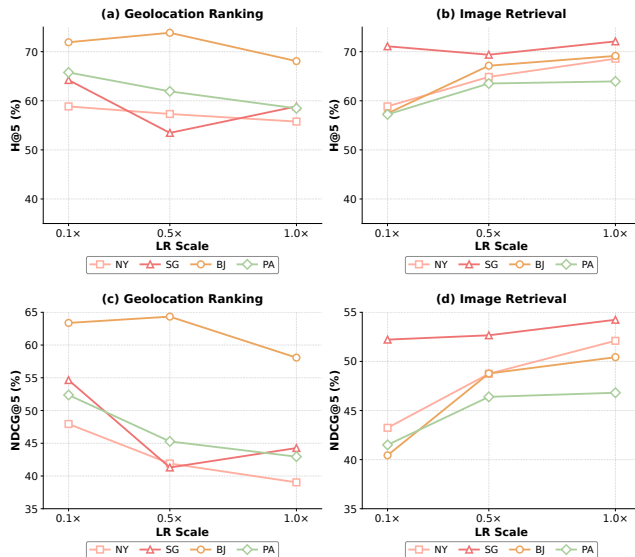


Figure 14: Effect of learning-rate scale between the Stage-2 graph encoder and LoRA adapters. (a,b) Hit@5 on geolocation ranking and image retrieval. (c,d) NDCG@5 on geolocation ranking and image retrieval. Smaller LR scales generally yield more stable improvements, while larger scales favor stronger graph–text coupling for retrieval.

K Inference efficiency

We report per-sample inference time on image retrieval. Graph conditioning increases latency from 2.9 s (image-only) to 11.0 s due to graph encoding and fusion.